Nondimensional shape optimisation of non-prismatic beams with sinusoidal lateral profile

Valerio De Biagi[1], Anna Reggio[2], Marco Martino Rosso[3], and Laura Sardone[4]

[1]DISEG, Department of Structural, Geotechnical and Building Engineering, Politecnico di Torino, Corso Duca degli Abruzzi, 24, Turin, 10129, Italy.

[2]DISEG, Department of Structural, Geotechnical and Building Engineering, Politecnico di Torino, Corso Duca degli Abruzzi, 24, Turin, 10129, Italy.

[3]DISEG, Department of Structural, Geotechnical and Building Engineering, Politecnico di Torino, Corso Duca degli Abruzzi, 24, Turin, 10129, Italy. Corresponding Author email: marco.rosso@polito.it

[4]Department of Civil Engineering and Architecture, Politecnico di Bari, Via Edoardo Orabona, 4, Bari, 70126, Italy

ABSTRACT

The present paper deals with the optimal design of non-prismatic beams, i.e. beams with variable cross-section. To set the optimisation problem, Euler-Bernoulli unshearable beam theory is considered and the elastica equation expressing the transverse displacement as a function of the applied loads is reformulated into a system of four differential equations involving kinematic components and internal forces. The optimal solution (in terms of volume) must satisfy two constraints: the maximum Von Mises equivalent stress must not exceed an (ideal) strength and the maximum vertical displacement is limited to a fraction of beam length. To evaluate the maximum equivalent stress in the beam, normal and shear stresses have been considered. The former evaluated through Navier formula, the latter through a formula derived from Jourawsky and holding for straight and untwisted beams with bi-symmetric variable cross-sections. The optimal

solutions as function of material unit weight, maximum strength and applied load are presented and discussed. It is shown that the binding constraint is usually represented by the maximum stress in the beam, and that applied load and strength affect the solution more than material unit weight. To maintain the generality of the solution, the nondimensionalisation according to Buckingham Π-theorem is implemented and a design abacus is proposed.

INTRODUCTION

In the last decades, non-prismatic beams have been widely adopted in the structural engineering field for civil, aerospace, and mechanical applications (El-Mezaini et al. 1991; Ascione et al. 2017; Vilar et al. 2022; Cucuzza et al. 2021; Sardone et al. 2020; Marano and Quaranta 2010; De Biagi et al. 2020; Magnucki et al. 2021). This type of beam is characterised by variable cross-section along its centroidal axis (Gere and Timoshenko 1997), bestowing it a strong interconnection among structural form, functionality, aesthetic and architectural requirements (Mercuri et al. 2020a). These features determined their everlasting success over the centuries, referring e.g. to monumental and historical architectures like Roman aqueducts and masonry arch structures. Non-prismatic elements have been extensively adopted even for infrastructures, e.g. for bridges and viaducts (Kozy and Tunstall 2007; Kaveh et al. 2022; Fiore et al. 2016; Muteb and Shaker 2017; Kaveh et al. 2020b; Zhou et al. 2019; Balduzzi et al. 2017), and buildings, such as double-tapered roof beams for industrial structures (Vilar et al. 2022; Bournas et al. 2014; McKinstray et al. 2016).

When dealing with prismatic beams, the classical Euler-Bernoulli beam theory holds, which neglects the shear deformation contribution and assumes the Navier hypothesis (Carpinteri 2013). Nonetheless, a more advanced theory is required to deal with non-prismatic beams, able to accurately and reliably capture the actual structural response. Therefore, in this research work, the Euler-Bernoulli unshearable beam theory was considered (Bertolini et al. 2019; Timoshenko and Goodier 1934). Recently, in the scientific literature, various mechanical models were proposed for non-prismatic beams. In (Medwadowski 1984), the authors proposed a solution of the differential equations for non-prismatic beams, denoted in that work as shear beams, considering the effect of shear deformations. In (Bulte 1992) the differential equation formulation of the deflection curve was presented as a multi-point boundary value problem. In (Romano 1996) analytical closed-form solutions were proposed for bending beams accounting for the shear deformation with non-prismatic parabolic profiles with both varying width and depth. In (Katsikadelis and Tsiatas 2003), the nonlinear large deflection analysis was conducted on the Euler-Bernoulli beam with variable stiffness with the analog equation method due to variable coefficients in the governing differential equations. In (Balduzzi et al. 2016), the authors analyse the compatibility and equilibrium of non-prismatic beams with a Timoshenko-like beam model, formulated as a system of six coupled ordinary differential equations (ODE). Cazzani et al. (Cazzani et al. 2016) proposed a Timoshenko beam model and a non-uniform rational B-splines (NURBS) interpolation to analyse curved beams with the isogeometric analysis (Hughes et al. 2005). In (Bertolini et al. 2019), the authors analysed the stress distribution in untwisted, straight, thin-walled beams with constant taper with rectangular and circular cross-section shapes. Most of the analytical approaches for non-prismatic beams proposed in the literature have been finally solved with the finite differences methods, even considering non-homogeneous conditions (Al-Azzawi and Emad 2020; Tuominen and Jaako 1992).

The non-prismatic geometry ensures great versatility for optimising specific structural aspects of interest (Rath et al. 1999; Sarma and Adeli 1998; Colin and MacRae 1984; Mercuri et al. 2020a; Kaveh et al. 2021), for instance, minimum material consumption, optimising structural performances, etc. In addition, the material used, e.g. concrete, steel, or wood (Maki and Kuenzi 1965), plays a crucial role in the shape and topology optimisation process due to distinct constitutive laws and possible changing behaviour in tension and compression. Furthermore, nowadays new materials and technologies such as additive manufacturing are opening new possibilities and promising research paths (Mercuri et al. 2020a). The problem of optimal design of non-prismatic beams has been studied quite extensively, implementing both gradient-based (Rao 2019) and gradient-free meta-heuristic algorithms (Resende et al. 2017; Plevris 2009), such as genetic algorithm (Cucuzza et al. 2021; Cucuzza et al. 2022; Biswal et al. 2017) or particle swarm optimisation algorithm (Rosso et al. 2022; Rosso et al. 2021). In (Luévanos-Rojas et al. 2020), the optimal design of reinforced concrete rectangular cross-section beams with straight haunches was analysed with the aim of reaching the minimum constitutive materials cost. In (Veenendaal et al. 2011), the optimal form-finding problem has been studied for the design of non-prismatic fabric-formed beams. The technical difficulties of traditional casting methods for these non-conventional variable curvature structures are nowadays partially overcome by leveraging innovative production technologies such as 3D printing and additive manufacturing (Asprone et al. 2018; Mercuri 2018; Costa et al. 2020). This latter aspect further nourishes the current relevance and contemporary of the present study on optimal variable-curvature non-prismatic solutions. In (Kaveh et al. 2020a; Kaveh et al. 2020b), the optimal seismic design of three-dimensional steel frames were carried on with the response spectrum analysis method. The same authors in a later study (Kaveh et al. 2021) analysed optimal performance-based reinforced concrete frames with objective function based on both cost and sustainability, expressed in terms of carbon dioxide emissions. Similarly, (Yavari et al. 2017) optimised environmental sustainability of non-prismatic slab frames bridge geometries. Recently, (Wang et al. 2021) proposed an innovation from a computational point of view for sequentially solving shape and topology optimization of beam structures, introducing the concept of 2.5D beam model than traditional 3D modeling. Basically, standard 1D beam elements are interconnected longitudinally,and, in every finite node, the section properties are retrieved from an additional bidimensional section model. The shape of the beam has been parametrically defined by non-uniform rational B-splines (NURBS) (Piegl and Tiller 1996).

In comparison to the literature previous studies, in the present work, the authors proposed an optimal design criterion for homogeneous constant width non-prismatic beams based on the *elastica* equation with a dimensionless perspective, eventually providing a design abacus. The main findings of the present work are summarised below:

- the minimum weight, or proportionally the minimum volume, optimisation problem was stated based on a dimensionless form of the *elastica* equation according to Buckhingam Π-theorem;
- the stress distributions considered Euler-Bernoulli unshearable beam theory (Bertolini et al.

2019);

- the constraints of the optimisation problem are expressed as Von Mises equivalent stress limitation and maximum limit vertical deflection limited to a fraction of beam length;
- the optimal solutions as a function of material unit weight, maximum strength, and applied load are presented in a design abacus graph form.

The current document is organised as follows. In Section 2, the analytical formulation of the *elastica* governing ODEs is presented, even illustrating the dimensionless procedure and the assumed stress distributions. The minimum volume (weight) optimisation problem statement is described in Section 3, showing that the non-prismatic variable beam depth profile is defined through an emptying sinusoidal function. Eventually, in Section 4 the optimal solutions as a function of material unit weight, maximum strength, and applied load are presented and discussed, finally delivering a useful design abacus encompassing the wide spectrum of design parameters analysed.

BEAM MODEL

A beam of length L, straight centerline and a variable cross-section is considered (Figure 1). A Cartesian coordinate system $(Oxyz)$ is introduced, setting: the origin O in the centroid of one of the end cross-sections; the x- and y-axes as the principal central axes of inertia of the cross-section; the z-axis along the beam centerline. We assume plane bending in the yz-plane, where the beam is subjected to distributed transverse load $q(z)$ and its deflection is described by transverse displacement $v(z)$. The constituting material is assumed to be homogeneous, isotropic and linear elastic with Young's modulus E.

Elastica equation

The beam is supposed of solid doubly-symmetric cross-section with variable depth $h(z)$. Based on the Euler-Bernoulli theory, beam deflection is governed by a fourth-order ODE, the *elastica* equation, which reads, for a variable cross-section beam,

$$\frac{\mathrm{d}}{\mathrm{d}z^2}\left[EJ(z)\frac{\mathrm{d}^2v(z)}{\mathrm{d}z^2}\right] = q(z), \tag{1}$$

where $J(z) = J_x(Z)$ is the area moment of inertia of the cross-section. By solving for differentiation and dividing both members by $EJ(z)$, the equation of the deflection curve reads

$$\frac{\mathrm{d}^4v(z)}{\mathrm{d}z^4} + 2\frac{\mathrm{d}^3v(z)}{\mathrm{d}z^3}\frac{\mathrm{d}J(z)}{\mathrm{d}z}\frac{1}{J(z)} + \frac{\mathrm{d}^2v(z)}{\mathrm{d}z^2}\frac{\mathrm{d}^2J(z)}{\mathrm{d}z^2}\frac{1}{J(z)} = \frac{q(z)}{EJ(z)}. \tag{2}$$

To give a more general description of the beam model, Buckingham Π-theorem is adopted (Barenblatt 1987) and a suitable nondimensionalisation is introduced by rescaling lengths by the beam span L and forces by EL^2. Nondimensional variables $\tilde{z} = z/L$ (with $\tilde{z} \in [0, 1]$), $\tilde{v} = v/L$ and functions $\tilde{J} = J/L^4$ and $\tilde{q} = q/EL$ are thus defined, while the derivative with respect to dimensional variable z is expressed as

$$\frac{\mathrm{d}}{\mathrm{d}z} = \frac{\mathrm{d}}{\mathrm{d}\tilde{z}}\frac{\mathrm{d}\tilde{z}}{\mathrm{d}z} = \frac{1}{L}\frac{\mathrm{d}}{\mathrm{d}\tilde{z}}. \tag{3}$$

Accordingly, Equation (2) can be rewritten as

$$\tilde{v}^{IV}(\tilde{z}) + 2\tilde{v}'''(\tilde{z})\frac{\tilde{J}'(\tilde{z})}{\tilde{J}(\tilde{z})} + \tilde{v}''(\tilde{z})\frac{\tilde{J}''(\tilde{z})}{\tilde{J}(\tilde{z})} = \frac{\tilde{q}(\tilde{z})}{\tilde{J}(\tilde{z})} \tag{4}$$

where the notation $(\cdot)'$ denotes the derivative with respect to nondimensional variable $\tilde{z}$.

First-order ODEs

Alternative to the *elastica* equation, Eqn. (1), the shear-bending problem of the variable cross-section beam can be formulated as a system of four first-order ODEs (Bulte 1992)

$$\begin{cases} \dfrac{dv}{dz} = -\phi(z), \\ \dfrac{d\phi}{dz} = \dfrac{M(z)}{EJ(z)}, \\ \dfrac{dM}{dz} = V(z), \\ \dfrac{dV}{dz} = -q(z), \end{cases} \tag{5}$$

Thanks to the functional $\mathbf{f}$, Eqn. (5) can be rewritten in vectorial notation as

$$\mathbf{w}'(z) = \mathbf{f}(z, \mathbf{w}), \tag{6}$$

where vector $\mathbf{w}$ has components $\mathrm{w}_1 = v(z)$, $\mathrm{w}_2 = \phi(z)$, $\mathrm{w}_3 = M(z)$ and $\mathrm{w}_4 = V(z)$, with ϕ the rotation of the cross-section (Figure 1). In this way, the variability of the cross-section is taken implicitly into account only by $J(z)$ and, due to the fact that all the equation are coupled, this is taken into account in the entire system avoiding to explicitly solve the fourth order equation depending by the derivative of the inertia. Moreover, in this way the solutions of the system directly represent shear, moment, rotation and deflection curves.

The distributed load $q(z)$ includes two contributions: (i) the beam self weight per unit length, equal to the product of the material unit weight γ by the cross-sectional area $A(z)$; (ii) the applied force per unit length q_0, assumed to be constant along the beam. It can thus be expressed as

$$q(z) = q_0(z) + \gamma A(z). \tag{7}$$

According to Buckhingam Π-theorem, it is possible to rewrite the system of Eqn. (5) as

$$\begin{cases} \dfrac{d\tilde{v}}{d\tilde{z}} = -\phi(\tilde{z}), \\ \dfrac{d\phi}{d\tilde{z}} = \dfrac{\tilde{M}(\tilde{z})}{\tilde{J}(\tilde{z})}, \\ \dfrac{d\tilde{M}}{d\tilde{z}} = \tilde{V}(\tilde{z}), \\ \dfrac{d\tilde{V}}{d\tilde{z}} = -\tilde{q}(\tilde{z}), \end{cases} \tag{8}$$

where

$$\tilde{M}(\tilde{z}) = \frac{M(\tilde{z})}{EL^2}, \tag{9}$$

$$\tilde{V}(\tilde{z}) = \frac{V(\tilde{z})}{EL^3}. \tag{10}$$

Accordingly, Eqn. (6), turns into

$$\tilde{\mathbf{w}}'(z) = \mathbf{f}(\tilde{z}, \tilde{\mathbf{w}}). \tag{11}$$

As previously illustrated, the normalized distributed load $\tilde{q}(\tilde{z})$ can be divided in two components as

$$\tilde{q}(\tilde{z}) = \tilde{\psi}_q(\tilde{z}) + \tilde{\psi}_\gamma \tilde{A}(\tilde{z}), \tag{12}$$

where

$$\tilde{\psi}_q(\tilde{z}) = \frac{q_0(\tilde{z})}{EL}, \tag{13}$$

$$\tilde{\psi}_\gamma = \frac{\gamma L}{E}, \tag{14}$$

and $\tilde{A}(\tilde{z}) = A(\tilde{z})/L^2.$ Considering a constant distributed applied force, Eqn. (12), turns into

$$\tilde{q}(\tilde{z}) = \tilde{\psi}_q + \tilde{\psi}_\gamma \tilde{A}(\tilde{z}). \tag{15}$$

Stress distributions

Beams with variable cross-section exhibit non-trivial stress distributions which differ from those predicted by the classical formulae of prismatic beam theory, in particular regarding shear stresses (Timoshenko 1956b; Oden 1981; Bruhns 2003). Under the assumption of plane bending, the beam is in a plane state of stress with $\sigma_x = \tau_{xy} = \tau_{zx} = 0$. Transverse normal stress σ_y, although non vanishing by equilibrium in non-prismatic beams, is generally small and can be neglected without appreciable error (Balduzzi et al. 2016). Distributions of normal stresses $\sigma := \sigma_z$ and shear stresses $\tau := \tau_{zy}$ acting on the cross-section are given as follows.

The distribution of normal stresses σ can be recovered by using the Navier flexure formula

$$\sigma(y, z) = \frac{M(z)}{J_x(z)} y \tag{16}$$

which holds with a good approximation for non-prismatic beams, provided the variation of the cross-section is not too rapid (Timoshenko 1956b; Boley 1963).

Conversely, the distribution of shear stresses τ is considerably altered compared to prismatic beams. In non-prismatic beams, shear stresses τ are dependent not only upon the internal shear force V, but also upon the internal axial force N and bending moment M, as well as on the changing rate of height and width of the beam (Bruhns 2003). This result follows from the equilibrium boundary condition on the beam's lateral surface, which requires the shear stress τ to be proportional to the normal stress σ due to the taper angle (Auricchio et al. 2015). Jourawsky's theory (Timoshenko 1956a) is consequently ineffective in predicting the actual shear stress distribution because (i) it violates the boundary equilibrium, (ii) cannot reproduce the correct distribution shape and magnitude and (iii) fails to identify the position and value of the maximum shear stress (Bruhns 2003; Paglietti and Carta 2009; Beltempo et al. 2015; Balduzzi et al. 2017; Mercuri et al. 2020b). In view of these considerations, we calculate the distribution of shear stresses by using the shear formula derived by Bertolini *et al.* (Bertolini et al. 2019, Equation 5), an extension of the Jourawsky formula holding for straight and untwisted beams with bi-symmetric variable cross-sections. Assuming null distributed couples applied to the beam and null internal axial force, the extended shear formula simplifies to

$$\tau(y,z) = \frac{1}{c(y,z)}\left[V(z)\frac{S^*(y,z)}{J(z)} + M(z)\frac{\mathrm{d}}{\mathrm{d}z}\left(\frac{S^*(y,z)}{J(z)}\right)\right], \tag{17}$$

where $c(y,z)$ is the cross-sectional width at the arbitrary level y where the shear stress τ is evaluated; $S^*(y,z) := S_x^*(y,z)$ is the first moment of area, with respect to the bending neutral axis x, of the cross-sectional region below the arbitrary level y. Specifically, for the rectangular cross-section, with constant width b and variable height $h(z)$, it holds

$$c(y,z) = b, \quad S^*(y,z) = \frac{b}{2}\left(\frac{h^2(z)}{4} - y^2\right), \quad J(z) = \frac{1}{12}bh^3(z), \tag{18}$$

and Eqn. (17) reads

$$\tau(y,z) = \frac{3}{2}\frac{1}{bh}\left[V(z)\left(1 - 4\frac{y^2}{h^2}\right) + M(z)\frac{\mathrm{d}h}{\mathrm{d}z}\left(-\frac{1}{h} + 12\frac{y^2}{h^3}\right)\right]. \tag{19}$$

OPTIMISATION PROBLEM

The optimisation problem tries to define the minimum volume which determines the minimum weight directly linked to the minimum usage of material respecting stress and deflection constraints (Cucuzza et al. 2021), which evaluations derive from structural analysis conducted with the system, Eqn. (8). Despite the minimization of the self-weight may not comprehensively cover all the numerous aspects for a general minimum cost design problem (Adeli and Sarma 2006), as a first approximation, and in the absence of precise requirements and prescription, it may be successfully employed as an indirect indicator of the cost, directly related to the minimum material consumption (Rao 2019; Cucuzza et al. 2021; Spillers and MacBain 2009). The minimization of self-weight also provides benefits for earthquake design situations (Plevris 2012; Rao 2019), for shells design loading (Adriaenssens et al. 2014), and also accounting for transportation and installation aspects especially involving precast elements solutions (Veenendaal 2008). In the dimensional problem, the stress constraints are treated in a simplified way adopting Von Mises criterion,

$$\sigma^2(z) + 3\tau^2(z) \leq \sigma_{id}^2. \tag{20}$$

where the ideal stress σ_{id} is assumed to be the yielding stress for an ideal material (same behaviour both in tension and in compression). Considering the above Von Mises stress constraint, Eqn. (20), and the specific forms for normal and shear stresses, Eqns. (16) and (19), respectively, it is possible to look for a dimensionless form to make consistency with the dimensionless system of Eqn. (8). In order to obtain a dimensionless stress it is sufficient to divide it by the elastic modulus E, and after some mathematical elaborations, it is possible to prove that

$$\tilde{\sigma}^2(\tilde{z}) + 3\tilde{\tau}^2(\tilde{z}) \leq \tilde{\psi}_{\sigma}^2, \tag{21}$$

in which a new dimensionless parameter is introduced, $\tilde{\psi}_{\sigma} = \sigma_{id}/E$. It is also possible to express the deflection constraint in a dimensionless form. Assuming a limit value of $v_{lim} = L/250$, the dimensionless deflection constraint is defined as

$$\tilde{v}(\tilde{z}) \leq \frac{1}{250}. \tag{22}$$

The above deflection limit value may be retrieved by general deformability requirements under service conditions contained in current structural codes regulations, e.g. the Eurocodes (EN1990 2002).

For evaluating the above-mentioned constraints of the optimisation problem herein investigated, various structural analyses have been conducted in order to account for possible multiple load cases conditions (Spillers and MacBain 2009; Cucuzza et al. 2022; Rao 2019). According to the basic principles of structural design (EN1990 2002), every structure has to be designed and assessed for the toughest loading conditions likely occurring in its lifespan. Therefore, it implies considering the envelope of the maximum actions' effects coming from different load combinations. For the sake of simplicity, in the current study, two different load conditions have been considered. The first load configuration accounts for the uniformly distributed load, as described in Eqn. (15), applied over the entire span length. The second load condition accounts for an asymmetric live load applied over the half-span length only. This latter configuration is usually more burdensome than the first load case for non-prismatic geometries, especially due to potential instability phenomena (Bazzucchi et al. 2017; Virgin et al. 2014). Since we are dealing with beam structures that may be employed, at different scales, both for buildings or bridges under uncertain locations of live loads (EN1990 2002), the asymmetric load condition must be applied on both the half-spans alternatively for accounting all the possible loading cases. In this sense, it should be expected that the optimal beam solution will still present a symmetric shape along the longitudinal axis. This optimal solution is expected stiffer profile than the one loaded with the first load case only, thus with a greater cross-section in general, but able to withstand both symmetric and asymmetric loading conditions.

Beam geometry definition

The previous constraints are applied to a doubly end-fixed beam having cross-section height that varies along the z-coordinate by way of an *emptying* function $\eta(z)$, given as a linear combination of sines

$$h(z) = h_0 - \eta(z) = h_0 - \sum_{i=1,3,5\ldots}^{N} \Delta h_i \sin\left(i\frac{\pi}{L}z\right), \tag{23}$$

where h_0 is the height of the end cross-sections, N is the number of harmonics combined in the emptying function and Δh_i is the amplitude of the i-th harmonic. A sketch of the beam is reported in Figure 2. The structural design principles and the load cases remarks mentioned in the previous section justify the authors' choice to focus only on the even sinusoidal harmonics in Eq.(23), thus delivering symmetrical beam profiles solutions. In this work, depending on the number of harmonics considered, we denote the beam with $N = 1$ as *one-lobe solution*, the one with $N = 3$ as *three-lobes solution*, and so forth. As an example, the height profile of the solution with three lobes is

$$h(z) = h_0 - \left[\Delta h_1 \sin\left(\frac{\pi}{L}z\right) + \Delta h_3 \sin\left(3\frac{\pi}{L}z\right)\right]. \tag{24}$$

In general, the volume of the emptied beam with sine emptying functions is equal to

$$V = \int_0^L A(z)dz \qquad \text{with} \quad A(z) = f(h(z)), \tag{25}$$

and therfore, the dimensionelss volume definition may be expressed as

$$\tilde{V} = \frac{V}{L^3} \tag{26}$$

For instance, detailing the above-mentioned Eqn. (25) for a rectrangular bysimmetrical cross-section it holds:

$$V = b\left[\int_0^L h(z)dz\right] = bL\left[h_0 - \sum_{i=1}^{N} \Delta h_i \frac{2}{i\pi}\right]. \tag{27}$$

According to the nondimensionalisation introduced in Section 2, it results

$$\tilde{h}(\tilde{z}) = \tilde{h}_0 - \tilde{\eta}(\tilde{z}) = \tilde{h}_0 - \sum_{i=1}^{N} \Delta\tilde{h}_i \sin(i\pi\tilde{z}) \tag{28}$$

and

$$\tilde{V} = \frac{V}{L^3} = \tilde{b}\left[\tilde{h}_0 - \sum_{i=1}^{N} \Delta\tilde{h}_i \frac{2}{i\pi}\right]. \tag{29}$$

Design vector and problem statement

Considering that the height of the beam must always be a positive number, i.e. $\tilde{h}(\tilde{z}) > 0$, we defined the dimensionless height of the end cross-section $\tilde{h}_0$ as the sum of a minimum height $\tilde{h}_{min}$, to be strictly positive, and the maximum emptying function, resulting in

$$\tilde{h}_0 = \tilde{h}_{min} + \max_{\tilde{z}\in[0,1]} \tilde{\eta}(\tilde{z}) \tag{30}$$

The design vector **D** collects the dimensionless values of the minimum height and the amplitudes coefficients of the sine function $\Delta\tilde{h}_i$. The optimization problem can be formulated in the following way

$$\begin{aligned} &\text{Find } \mathbf{D} = \{\tilde{h}_{min}; \Delta\tilde{h}_i\}_{i=1,3,5...} \text{ such that} \\ &\min \tilde{V}(\mathbf{D}) \\ &\text{s.t. } \tilde{\sigma}^2(\tilde{z}) + 3\tilde{\tau}^2(\tilde{z}) \leq \tilde{\psi}_\sigma^2, \\ &\tilde{v}(\tilde{z}) \leq \frac{1}{250} \end{aligned} \tag{31}$$

Thanks to the procedure previously described and implemented in Matlab, the optimal geometry of beams with different combinations of parameters ψ_q, ψ_γ and ψ_σ was investigated. The dimensionless form allows covering all the possible situations for the specific problem parameters values such as the span length, geometric and material properties included in the aforementioned parameters.

For the sake of better controlling the optimization process, limiting the mathematical topology complexity of the search space, and in order to avoid an excessive over-parametrization of the beam's shape longitudinal profile, the authors studied the optimization process using the number of sine-emptying lobes as a fixed parameter rather than a design variable. Specifically, the authors provided a detailed comparison and discussion of four different structural configurations, i.e. from one-lobe to seven-lobes. For a number of lobes greater than seven-lobes, the authors observed that the influence of higher lobes was practically negligible compared to the increase of the beam's shape profile complexity.

RESULTS AND DISCUSSION

In this section, the results of optimization analyses for a beam with rectangular cross-section are presented. The structural analyses have been conducted under two different load conditions. The first load configuration accounts for the uniformly distributed load, as described in Eqn. (15), applied over the entire span length. The second load condition accounts for an asymmetric live load applied over the half-span length only. This latter configuration is usually more burdensome than the first load case for non-prismatic geometries, especially due to potential instability phenomena

(Bazzucchi et al. 2017; Virgin et al. 2014). Furthermore, in the current study, point loads have not been explicitly considered since they are properly representative of specific design situations, see e.g. (Yang et al. 2022). Nonetheless, the current methodology may account for point loads as well by implementing equivalent distributed loads over a short finite length, simulating its actual load footprint.

Several analyses were carried to determine the influence of the number of lobes on the optimal beam solution and to highlight the effects of the maximum allowable stress level and material unit weight. A design abacus is proposed to summarise the results. The optimisation problem was implemented in a Matlab code and solved with the *fmincon* function provided within the *Optimization Toolbox* package (MATLAB Optimization Toolbox). The input parameters of the fmincon function are the objective function defined in Eqn. (29) and the non-linear constraints defined in Eqs. (21)-(22), both summarized in the optimisation problem statement in Eqn. (31). The solver algorithm option has been set to the well-acknowledged and efficient nonlinear programming method named sequential quadratic programming (SQP) (Schittkowski 1986). This gradient-based iterative method is based on quasi-Newton approximation of the Hessian of the Lagrangian function for constrained optimization problems (Rao 2019), which translates in the resolution of quadratic programming subproblems forming an active set strategy for a line search procedure (Biggs 1975; Han 1977; Powell 2006; Powell 1978). Since the current implementation requires strict feasibility with respect to constraints, it implements an automatic adaptation of the finite difference gradient step along the line search, and due to the quasi-Netwon approximation of the Hessian, any second-order eigenvalue sensitivity is not strictly necessary (Li et al. 2016).

Influence of the number of lobes

Figure 3 shows the optimal solutions (in grey) considering the material and geometric properties reported in Table 1. Four different configurations were compared, from one-lobe to seven-lobes, i.e. considering $N = 1, 3, 5, 7$. For each case, the components of vector $\tilde{\mathbf{w}}$, i.e. nondimensional displacement $\tilde{v}$, rotation ϕ, bending moment $\tilde{M}$ and shear $\tilde{V}$ are reported in the top subplots. The displacement plot (top left) includes a horizontal red line denoting the limit value, i.e. 1/250. The bottom plot refers to the maximum Von Mises stress along the beam and includes (in red) the threshold ψ_σ.

For all the examined cases, the maximum stress in the beam represents the most strict (binding) constraint. Table 2 reports the values of the components of the design vector $\mathbf{D}$. Comparing the various solutions, it results that increasing the number of lobes reduces the volume of the optimal beam. The presence of two parts with limited height, which emerges for $N = 3$ and is further highlighted for $N = 5, 7$, implies larger rotations and, by consequence, increased displacements. The number of lobes in the solution affects Von Mises equivalent stress. For $N = 1$, the maximum stresses are observed at beam ends and at midspan, where heights h_0 and h_{min} can be optimised. A different trend is noted for $N = 3$, where the maximum stress occurs at 1/6 and 5/6 of beam length, roughly. Considering the area below the stress curve as an ideal measure of the material exploitation rate, it results that the best use is obtained when the stress level tends to the threshold value in any section of the beam. Comparing the solutions with different number of lobes, it clearly emerges that the larger the number of lobes, the better the exploitation rate. Five- and seven-lobes solutions produce similar maximum vertical displacements, but different material exploitation, in particular in the first and last sixth of the beam. In detail, $N = 7$ solution exhibits a stress plateau in the first and last part of the beam. The similarity in five- and seven-lobes solutions emerges in analysing the components of the design vector reported in Table 2. Checking the $\tilde{V}$ column, i.e. the values of the objective function, it results that the reduction in the optimal volume (target of the optimisation) is more evident up to $N = 5$, while for $N = 7$, the resulting $\tilde{V}$ is close to the five-lobes solution. As a conclusion, three-lobes and five-lobes represent feasible solutions for fixed-fixed beams with uniformly distributed load.

For the sake of completeness, other boundary conditions should be analysed in future studies since the herein-presented double fixed condition is mainly representative of concrete structures. Indeed, the authors preliminary tested the current optimization procedure considering other beam boundary conditions, in particular the double-hinged one. However, the obtained optimal results appear not relevant for the scope of the current study, and they have not been herein reported. Nonetheless, it is worth reminding that for other structural materials, such as steel or timber, the semi-rigid restraints condition is the actual one. A proper embedding of these aspects is out of the scope of the current manuscript and may require future deeper investigations. Indeed, special attention should be paid to the specific technical choice adopted for the restrain joints, which affects their rotational stiffness capacity on the moment rotation plane (Daniūnas and Urbonas 2008; Du et al. 2022).

Influence of the maximum stress

Three-lobes solution was adopted for assessing the effect of maximum stress on the optimal beam height profile. The optimisation problem of Eqn. (31) was solved considering geometric and load parameters reported in Table 3. To highlight the dependency of the optimal solution on the value of the stress parameter ψ_σ, three different values were considered, i.e. $\psi_\sigma = 3.33 \times 10^{-4}, 6.66 \times 10^{-4}$, and 1×10^{-3}. These correspond to ideal stresses σ_{id} of 10, 20 and 30 MPa. Figure 4 shows the optimal solutions for the three stress levels and Table 4 details the amplitudes of the sine functions and the value of the objective function. Comparing stress and displacement curves of the three solutions it emerges that different trends emerge. For low stress levels, say $\psi_\sigma = 3.33 \times 10^{-4}$, the relevant constraint for the optimal solution is represented by the maximum allowable stress itself. For high stresses, $\psi_\sigma = 1 \times 10^{-3}$, the maximum displacement is the binding term. For medium stresses, $\psi_\sigma = 6.66 \times 10^{-4}$, both constraints are relevant for the optimal solution.

As a matter of evidence, the optimal solution would benefit in terms of volume of material if the maximum allowable stress level increases. To measure such benefit, Table 4 reports in the values of the nondimensional volume $\tilde{V}$. The change of ψ_σ affects the value of the objective function in a nonlinear manner, with no direct relationship between the value of ψ_σ and $\tilde{V}$. To address such issue, a parametric analysis was performed to highlight the specific binding constraint and study the value of the objective function. Figure 5 details the results in term of $\tilde{V}$ (contour lines) and relevant constraint in the optimisation (coloured bullets) for $N = 3$, $\psi_\gamma = 8.33 \times 10^{-6}$ and $\tilde{b} = 0.05$. The load parameter ψ_q varies in the range from 3.33×10^{-8} to 1.67×10^{-7} that corresponds to a distributed load between 10 and 100 kN/m (the remaining variables are those reported in Table 3). The stress parameter ψ_σ varies in the range from 3.33×10^{-4} to 1×10^{-3}. It is shown that, for the larges part of the investigated cases, the binding constraint is represented by the maximum stress in the beam (similarly to what shown in Figure 4.a). For large maximum stresses, the relevant condition is the maximum displacement, highlighted with blue bullets. The transition between the two limit conditions depends on the value of the distributed load, in particular for $\psi_\sigma > 6 \times 10^{-4}$. Observing the trends of $\tilde{V}$ in the black contour plot, it is seen that for high ψ_σ, the optimal volume depends on the external load, only, as the beam shape is constrained by the maximum displacement. For high values of ψ_q, the maximum stress controls the optimal volume.

Influence of material unit weight

To study the influence of the unit weight of the material constituting the beam, three scenarios were considered and compared. The solution reported in Figure 4.c obtained for $\psi_\gamma = 8.33 \times 10^{-6}, \psi_q = 3.33 \times 10^{-8}$ and $\psi_\sigma = 1 \times 10^{-3}$ is considered as reference for the analysis. Two additional cases were considered, keeping fixed all the parameters except ψ_γ which is halved and doubled. The results of the optimisation are reported in Table 5. It is found that the modification of ψ_γ affects in a limited way the values of the amplitudes of the optimal solution, nor the volume of the beam, that is, its weight. To understand the reason of such trend, it is necessary to consider the total weight of the beam, namely G, computed as $G = \gamma V$, which can be expressed in nondimensional form as

$$\tilde{G} = \psi_\gamma \tilde{V}. \tag{32}$$

The total applied load Q is computed as $Q = q_0 L$, which can be further expressed as

$$\tilde{Q} = \psi_q. \tag{33}$$

For all the analysed cases, the result of Eqn. (32) (reported in the seventh column of Table 5), is smaller than ψ_q (3.33×10^{-8}), showing that the dead load is not relevant in the solution.

Design abacus

The analyses performed highlighted that three- and five-lobes solutions provide good results for the minization of the objective function. Considering the parameters describing material weight, load and maximum allowable stress, it was shown that ψ_q and ψ_σ play a relevant role in the optimal solution, while the parameter associated to the unit weight ψ_γ has a secondary importance since it slightly affects the optimal design. To let the solution the more general as possible, various combination of real construction materials, geometries and loads were considered. A summary of these is reported in Table 6; among all the cases, ψ_γ varies between 3.71×10^{-7} and 8.33×10^{-6}, ψ_σ varies between 1.00×10^{-3} and 3.75×10^{-3}, and ψ_q varies between 9.52×10^{-10} and 6.25×10^{-6}. The design abacus, which would serve for defining the optimal height profile of the beam, was formulated for a fixed value of $\psi_\gamma = 1\times10^{-6}$, ψ_σ in the range 0.5×10^{-3} to 1.5×10^{-3} (3 values) and ψ_q in the range 4×10^{-8} to 4×10^{-6} (in 7 logaritmically equally spaced values), trying to represent the possible materials, beam lengths and loads configurations. The nondimensional beam width is $\tilde{b} = 0.05$.

Table 7 reports the optimal values of the design vector and the corresponding $\tilde{V}$. It results that $\tilde{V}$ is in the range 0.001 to 0.0085, roughly. In general, the values of h_{min} and the absolute values of the amplitudes of the sine function $\Delta\tilde{h}_1$, $\Delta\tilde{h}_3$ and $\Delta\tilde{h}_5$ increase for increasing ψ_q. Besides, the increase of ψ_σ causes a reduction of the terms. These trends reflect the findings of the specific studies reported in the previous sections.

Figure 6 shows the height profiles of the optimal beams. The scale in Y-axes are kept constant in all the plots for a better understanding of the effects of the parameters on the optimal solution. The results of Table 7 can be used for the design of real beams: the design values, i.e., the minimum height and the sine amplitudes can be determined by interpolation for a given ψ_σ and ψ_q.

CONCLUSIONS

The present paper deals with the optimal design of beams with variable cross-section. To this aim, Euler-Bernoulli beam theory has been adopted. The fourth order elastica equation has been rewritten according to the formulation proposed by Bulte as a system of four differential equations. According to Buckinham Π-theorem, a nondimensionalisation has been done to let the solution as general as possible. The loads acting of the beam are the self weight and a distributed line load. The minimum volume (weight) solution must satisfy two constraints: the maximum Von

Mises equivalent stress must not exceed an (ideal) strength and the maximum vertical displacement is limited to a fraction (1/250) of beam length. To evaluate the maximum equivalent stress in the beam, normal and shear stresses have been considered. The former evaluated through Navier formula, the latter through a formula derived from Jourawsky and holding for straight and untwisted beams with bi-symmetric variable cross-sections. The optimisation problem has focused on a beam with fixed-fixed ends subjected to a uniformly distributed load. To create the variable height profile, an emptying function resulting as a combination of sine functions with different amplitudes has been introduced. For the sake of completeness, other boundary conditions should be analysed in future studies. The double fixed condition is mainly representative of concrete structures, whereas for e.g. steel or timber structures, the semi-rigid condition is the actual one. However, considering these aspects may require future investigations accounting for the specific technical choice adopted for the restrain joints, thus affecting their rotational stiffness capacity (Daniūnas and Urbonas 2008; Du et al. 2022).

The parametric analyses showed that:

- the choice of the number of sines in the emptying function that describes the shape of the beam, is relevant up to $N = 5$, i.e., a five-lobes solution. For finer solution, for examples, seven-lobes solution, there is not an improvement in the optimal solution in terms of minimum weight;
- the maximum stress in the material influences the binding constraint. In general, it has been noted that the stress constraint is relevant for the optimal solution for the large majority of cases. The displacement constraint affects the solution for low external loads and high strength;
- material unit weight does not affect the optimal solution as the total weight of the beam is smaller that the total applied load. For this reason, the variability of the material can be avoided in a preliminary design of a beam.

A design abacus with a profiles plot encompassing the wide spectrum of design parameters has been proposed to help in the design of an optimal five-lobes solution. The findings of the present paper would serve for the design of beams optimised with respect to weight. It should be emphasized that the current optimization problem statement in Eqn. (31) may be further refined, e.g. peculiarly referring to more detailed constraints derived from actual structural codes based on the specific constitutive materials adopted (NTC 2018; EN1990 2002). Furthermore, traditional casting methods for concrete non-prismatic beams with variable curvature profiles are still challenging (Veenendaal et al. 2011), especially for rebar placing operations, and often lead to more expensive solutions than classical alternatives. Nevertheless, in the novel panorama of additive manufacturing and 3D printing (Costa et al. 2020; Mercuri 2018), the herein-studied structural solution is already becoming more feasible, revolutionizing the current construction industry. Therefore, future research efforts will concern the numerous aspects related to promising 3D printing casting solutions, e.g. involving innovative and printing-technologically compatible materials, life cycle assessment, and non-prismatic beams industrialization among others (Costa et al. 2020; Gregori et al. 2019; Fiore et al. 2014; Asprone et al. 2018).

Data Availability Statement

All data, models, or code that support the findings of this study are available from the corresponding author upon reasonable request.

Acknowledgments

This research was supported by project MSCA-RISE-2020 Marie Skłodowska-Curie Research and Innovation Staff Exchange (RISE) - ADDOPTML (ntua.gr) “ADDitively Manufactured OPTimized Structures by means of Machine Learning" (No: 101007595)

REFERENCES

Adeli, H. and Sarma, K. C. (2006). *Cost optimization of structures: fuzzy logic, genetic algorithms, and parallel computing*. John Wiley & Sons.

Adriaenssens, S., Block, P., Veenendaal, D., and Williams, C. (2014). *Shell structures for architecture: form finding and optimization*. Routledge.

Al-Azzawi, A. A. and Emad, H. (2020). “Numerical analysis of nonhomogeneous and nonprismatic members under generalised loadings.” *IOP Conference Series: Materials Science and Engineering*, Vol. 671, IOP Publishing, 012097.

Ascione, L., Berardi, V., Feo, L., Fraternali, F., and Tralli, A. M. (2017). “Non-prismatic thin-walled beams: critical issues and effective modeling.” *Proc. of AIMETA 2017 XXIII Conference (September 4–7, 2017, Salerno, Italy), Salerno*, 301–308.

Asprone, D., Auricchio, F., Menna, C., and Mercuri, V. (2018). “3d printing of reinforced concrete elements: Technology and design approach.” *Construction and Building Materials*, 165, 218–231.

Auricchio, F., Balduzzi, G., and Lovadina, C. (2015). “The dimensional reduction approach for 2D non-prismatic beam modelling: A solution based on Hellinger-Reissner principle.” *International Journal of Solids and Structures*, 63, 264–276.

Balduzzi, G., Aminbaghai, M., Sacco, E., Füssl, J., Eberhardsteiner, J., and Auricchio, F. (2016). “Non-prismatic beams: A simple and effective Timoshenko-like model.” *International Journal of Solids and Structures*, 90, 236–250.

Balduzzi, G., Hochreiner, G., and Füssl, J. (2017). “Stress recovery from one dimensional models for tapered bi-symmetric thin-walled I beams: Deficiencies in modern engineering tools and procedures.” *Thin-Walled Structures*, 119, 934–945.

Barenblatt, G. I. (1987). *Dimensional analysis*. CRC Press.

Bazzucchi, F., Manuello, A., and Carpinteri, A. (2017). “Instability load evaluation of shallow imperfection-sensitive structures by form and interaction parameters.” *European Journal of Mechanics-A/Solids*, 66, 201–211.

Beltempo, A., Balduzzi, G., Alfano, G., and Auricchio, F. (2015). “Analytical derivation of a general 2D non-prismatic beam model based on the Hellinger-Reissner principle.” *Engineering Structures*, 101, 88–98.

Bertolini, P., Eder, M., Taglialegne, L., and Valvo, P. (2019). “Stresses in constant tapered beams with thin-walled rectangular and circular cross sections.” *Thin-Walled Structures*, 137, 527–540.

Biggs, M. (1975). "Constrained minimization using recursive quadratic programming." *Towards global optimization*.

Biswal, A. R., Roy, T., and Behera, R. K. (2017). "Optimal vibration energy harvesting from non-prismatic axially functionally graded piezolaminated cantilever beam using genetic algorithm." *Journal of Intelligent Material Systems and Structures*, 28(14), 1957–1976.

Boley, B. (1963). "On the Accuracy of the Bernoulli-Euler Theory for Bemas of Variable Section." *Journal of Applied Mechanics ASME*, 30(3), 373–378.

Bournas, D. A., Negro, P., and Taucer, F. F. (2014). "Performance of industrial buildings during the emilia earthquakes in northern italy and recommendations for their strengthening." *Bulletin of Earthquake Engineering*, 12(5), 2383–2404.

Bruhns, O. T. (2003). *Advanced Mechanics of Solids*. Springer, Berlin.

Bulte, C. (1992). "The differential equation of the deflection curve." *International Journal of Mathematical Education in Science and Technology*, 23(1), 51–63.

Carpinteri, A. (2013). *Structural mechanics fundamentals*. Taylor & Francis, Boca Raton, FL.

Cazzani, A., Malagù, M., and Turco, E. (2016). "Isogeometric analysis of plane-curved beams." *Mathematics and Mechanics of Solids*, 21(5), 562–577.

Colin, M. and MacRae, A. (1984). "Optimization of structural concrete beams." *Journal of structural engineering*, 110(7), 1573–1588.

Costa, E., Shepherd, P., Orr, J., Ibell, T., and Oval, R. (2020). "Automating concrete construction: Digital design of non-prismatic reinforced concrete beams." *Second RILEM International Conference on Concrete and Digital Fabrication: Digital Concrete 2020 2*, Springer, 863–872.

Cucuzza, R., Rosso, M. M., Aloisio, A., Melchiorre, J., Giudice, M. L., and Marano, G. C. (2022). "Size and shape optimization of a guyed mast structure under wind, ice and seismic loading." *Applied Sciences*, 12(10), 4875.

Cucuzza, R., Rosso, M. M., and Marano, G. C. (2021). "Optimal preliminary design of variable section beams criterion." *SN Applied Sciences*, 3(8), 1–12.

Daniūnas, A. and Urbonas, K. (2008). "Analysis of the steel frames with the semi-rigid beam-to-beam and beam-to-column knee joints under bending and axial forces." *Engineering structures*, 30(11), 3114–3118.

De Biagi, V., Chiaia, B., Marano, G. C., Fiore, A., Greco, R., Sardone, L., Cucuzza, R., Cascella, G. L., Spinelli, M., and Lagaros, N. D. (2020). "Series solution of beams with variable cross-section." *Procedia Manufacturing*, 44, 489–496.

Du, H., Zhao, P., Wang, Y., and Sun, W. (2022). "Seismic experimental assessment of beam-through beam-column connections for modular prefabricated steel moment frames." *Journal of Constructional Steel Research*, 192, 107208.

El-Mezaini, N., Balkaya, C., and Çitipitio g ˇ lu, E. (1991). "Analysis of frames with nonprismatic members." *Journal of Structural Engineering*, 117(6), 1573–1592.

EN1990 (2002). "Eurocode: Basis of structural design." *United Kingdom: British Standards Institute*.

Fiore, A., Marano, G. C., Marti, C., and Molfetta, M. (2014). "On the fresh/hardened properties of cement composites incorporating rubber particles from recycled tires." *Advances in Civil Engineering*, 2014.

Fiore, A., Quaranta, G., Marano, G. C., and Monti, G. (2016). "Evolutionary polynomial regression–based statistical determination of the shear capacity equation for reinforced concrete beams without stirrups." *Journal of Computing in Civil Engineering*, 30(1), 04014111.

Gere, J. M. and Timoshenko, S. (1997). "Mechanics of materials. ed." *Boston, MA: PWS*.

Gregori, A., Castoro, C., Marano, G. C., and Greco, R. (2019). "Strength reduction factor of concrete with recycled rubber aggregates from tires." *Journal of Materials in Civil Engineering*, 31(8), 04019146.

Han, S.-P. (1977). "A globally convergent method for nonlinear programming." *Journal of optimization theory and applications*, 22(3), 297–309.

Hughes, T. J., Cottrell, J. A., and Bazilevs, Y. (2005). "Isogeometric analysis: Cad, finite elements, nurbs, exact geometry and mesh refinement." *Computer methods in applied mechanics and engineering*, 194(39-41), 4135–4195.

Katsikadelis, J. T. and Tsiatas, G. (2003). "Large deflection analysis of beams with variable stiffness." *Acta Mechanica*, 164(1), 1–13.

Kaveh, A., Kabir, M., and Bohlool, M. (2020a). "Optimum design of three-dimensional steel frames with prismatic and non-prismatic elements." *Engineering with Computers*, 36(3), 1011–1027.

Kaveh, A., Mottaghi, L., and Izadifard, A. (2022). "Parametric study: cost optimization of non-prismatic reinforced concrete box girder bridges with different number of cells." *Iran University of Science & Technology*, 12(1), 1–14.

Kaveh, A., Mottaghi, L., and Izadifard, R. (2020b). "Sustainable design of reinforced concrete frames with non-prismatic beams." *Engineering with Computers*, 1–18.

Kaveh, A., Mottaghi, L., and Izadifard, R. (2021). "An integrated method for sustainable performance-based optimal seismic design of rc frames with non-prismatic beams." *Scientia Iranica*, 28(5), 2596–2612.

Kozy, B. and Tunstall, S. (2007). "Stability analysis and bracing for system buckling in twin i-girder bridges." *Bridge Structures*, 3(3, 4), 149–163.

Li, P., Qi, J., Wang, J., Wei, H., Bai, X., and Qiu, F. (2016). "An sqp method combined with gradient sampling for small-signal stability constrained opf." *IEEE Transactions on Power Systems*, 32(3), 2372–2381.

Luévanos-Rojas, A., López-Chavarría, S., Medina-Elizondo, M., and Kalashnikov, V. V. (2020). "Optimal design of reinforced concrete beams for rectangular sections with straight haunches." *Revista de la construcción*, 19(1), 90–102.

Magnucki, K., Magnucka-Blandzi, E., Milecki, S., Goliwas, D., and Wittenbeck, L. (2021). "Free flexural vibrations of homogeneous beams with symmetrically variable depths." *Acta Mechanica*, 232(11), 4309–4324.

Maki, A. and Kuenzi, E. W. (1965). *Deflection and stresses of tapered wood beams*, Vol. 34. US Department of Agriculture, Forest Service, Forest Products Laboratory, Madison, WI.

Marano, G. C. and Quaranta, G. (2010). "A new possibilistic reliability index definition." *Acta mechanica*, 210(3-4), 291–303.

MATLAB Optimization Toolbox. “Matlab optimization toolbox. The MathWorks, Natick, MA, USA.

McKinstray, R., Lim, J. B., Tanyimboh, T. T., Phan, D. T., and Sha, W. (2016). “Comparison of optimal designs of steel portal frames including topological asymmetry considering rolled, fabricated and tapered sections.” *Engineering Structures*, 111, 505–524.

Medwadowski, S. J. (1984). “Nonprismatic shear beams.” *Journal of Structural Engineering*, 110(5), 1067–1082.

Mercuri, V. (2018). “Form and structural optimization: from beam modeling to 3d printing reinforced concrete members.” Ph.D. thesis, Università degli Studi di Pavia, Pavia.

Mercuri, V., Balduzzi, G., Asprone, D., and Auricchio, F. (2020a). “Structural analysis of non-prismatic beams: Critical issues, accurate stress recovery, and analytical definition of the finite element (FE) stiffness matrix.” *Engineering Structures*, 213, 110252.

Mercuri, V., Balduzzi, G., Asprone, D., and Auricchio, F. (2020b). “Structural analysis of non-prismatic beams: Critical issues, accurate stress recovery, and analytical definition of the Finite Element (FE) stiffness matrix.” *Engineering Structures*, 213, 110252.

Muteb, H. H. and Shaker, M. S. (2017). “Strength of non-prismatic composite self-compacting concrete.” *The 2017 World Congress on Advances in Structural Engineering and Mechanics (ASEM17)*, 1–110.

NTC (2018). “Aggiornamento delle norme tecniche per le costruzioni.” *Gazzetta Ufficiale Serie Generale*, (42).

Oden, J. (1981). *Mechanics of Elastic Structures*. McGraw-Hill, New York, USA.

Paglietti, A. and Carta, G. (2009). “Remarks on the Current Theory of Shear Strength of Variable Depth Beams.” *The Open Civil Engineering Journal*, 3(1), 28–33.

Piegl, L. and Tiller, W. (1996). *The NURBS book*. Springer Science & Business Media.

Plevris, V. (2009). “Innovative computational techniques for the optimum structural design considering uncertainties.” Ph.D. thesis, Εθνικό Μετσόβιο Πολυτεχνείο (ΕΜΠ). Σχολή Πολιτικών Μηχανικών. Τομέας ?, National Technical University Of Athens.

Plevris, V. (2012). *Structural seismic design optimization and earthquake engineering: formulations and applications: formulations and applications*. IGI Global.

Powell, M. J. (1978). "The convergence of variable metric methods for nonlinearly constrained optimization calculations." *Nonlinear programming 3*, Elsevier, 27–63.

Powell, M. J. (2006). "A fast algorithm for nonlinearly constrained optimization calculations." *Numerical Analysis: Proceedings of the Biennial Conference Held at Dundee, June 28–July 1, 1977*, Springer, 144–157.

Rao, S. S. (2019). *Engineering optimization: theory and practice*. John Wiley & Sons, NY.

Rath, D., Ahlawat, A., and Ramaswamy, A. (1999). "Shape optimization of rc flexural members." *Journal of Structural Engineering*, 125(12), 1439–1446.

Resende, M. G., Martí, R., and Pardalos, P. (2017). "Handbook of heuristics.

Romano, F. (1996). "Deflections of Timoshenko beam with varying cross-section." *International Journal of Mechanical Sciences*, 38(8-9), 1017–1035.

Rosso, M. M., Cucuzza, R., Aloisio, A., and Marano, G. C. (2022). "Enhanced multi-strategy particle swarm optimization for constrained problems with an evolutionary-strategies-based unfeasible local search operator." *Applied Sciences*, 12(5), 2285.

Rosso, M. M., Cucuzza, R., Di Trapani, F., and Marano, G. C. (2021). "Nonpenalty machine learning constraint handling using pso-svm for structural optimization." *Advances in Civil Engineering*, 2021.

Sardone, L., Greco, R., Fiore, A., Moccia, C., De Tommasi, D., and Lagaros, N. D. (2020). "A preliminary study on a variable section beam through algorithm-aided design: a way to connect architectural shape and structural optimization." *Procedia Manufacturing*, 44, 497–504.

Sarma, K. C. and Adeli, H. (1998). "Cost optimization of concrete structures." *Journal of structural engineering*, 124(5), 570–578.

Schittkowski, K. (1986). "Nlpql: A fortran subroutine solving constrained nonlinear programming problems." *Annals of operations research*, 5, 485–500.

Spillers, W. R. and MacBain, K. M. (2009). *Structural optimization*. Springer Science & Business

Media.

Timoshenko, S. (1956a). *Strength of Materials - Part I Elementary Theory and Problems*. D. Van Nostrand, Princeton, New Jersey, USA, third edition.

Timoshenko, S. (1956b). *Strength of Materials - Part II Advanced Theory and Problems*. D. Van Nostrand, Princeton, New Jersey, USA, third edition.

Timoshenko, S. P. and Goodier, J. N. (1934). *Theory of Elasticity*. McGraw-Hill, NY.

Tuominen, P. and Jaako, T. (1992). “Generation of beam elements using the finite difference method.” *Computers & structures*, 44(1-2), 223–227.

Veenendaal, D. (2008). “Evolutionary optimization of fabric formed structural elements: Bridging the gap between computational optimization and manufacturability.

Veenendaal, D., Coenders, J., Vambersky, J., and West, M. (2011). “Design and optimization of fabric-formed beams and trusses: evolutionary algorithms and form-finding.” *Structural Concrete*, 12(4), 241–254.

Vilar, M., Hadjiloizi, D., Khaneh Masjedi, P., and Weaver, P. (2022). “Stress recovery of laminated non-prismatic beams under layerwise traction and body forces.” *International Journal of Mechanics and Materials in Design*, 18(3), 719–741.

Virgin, L., Wiebe, R., Spottswood, S., and Eason, T. (2014). “Sensitivity in the structural behavior of shallow arches.” *International Journal of Non-Linear Mechanics*, 58, 212–221.

Wang, Z., Suiker, A. S., Hofmeyer, H., van Hooff, T., and Blocken, B. (2021). “Sequentially coupled shape and topology optimization for 2.5 d and 3d beam models.” *Acta Mechanica*, 232, 1683–1708.

Yang, J., Xia, J., Zhang, Z., Zou, Y., Wang, Z., and Zhou, J. (2022). “Experimental and numerical investigations on the mechanical behavior of reinforced concrete arches strengthened with uhpc subjected to asymmetric load.” *Structures*, Vol. 39, Elsevier, 1158–1175.

Yavari, M. S., Du, G., Pacoste, C., and Karoumi, R. (2017). “Environmental impact optimization of reinforced concrete slab frame bridges.” *Journal of Civil Engineering and Architecture*, 11(4), 313–324.

Zhou, M., Shang, X., Hassanein, M. F., and Zhou, L. (2019). “The differences in the mechanical performance of prismatic and non-prismatic beams with corrugated steel webs: A comparative research.” *Thin-Walled Structures*, 141, 402–410.

List of Tables

TABLE 1. Material and geometric properties for the analysis related to the number of lobes.

γ	25 kN/m^3
E	30 GPa
L	10 m
q_0	20 kN/m
σ_{id}	20 MPa
$\tilde{b}$	0.05
ψ_γ	8.33×10^{-6}
ψ_q	6.66×10^{-8}
ψ_σ	6.66×10^{-4}

TABLE 2. Optimal design values related to the cases of Figure 3.

N	$\tilde{h}_{min}$	$\Delta\tilde{h}_1$	$\Delta\tilde{h}_3$	$\Delta\tilde{h}_5$	$\Delta\tilde{h}_7$	$\tilde{V}$
1	0.0151	0.0231				1.17×10^{-3}
3	0.0157	0.0301	0.0055			1.07×10^{-3}
5	0.0119	0.0262	0.0040	-0.0026		9.93×10^{-4}
7	0.0122	0.0262	0.0040	-0.0026	0.00028	9.95×10^{-4}

TABLE 3. Material and geometric properties for the analysis related to the effect of maximum material stress.

γ	25 kN/m^3
E	30 GPa
L	10 m
q_0	10 kN/m
$\tilde{b}$	0.05
ψ_γ	8.33×10^{-6}
ψ_q	3.33×10^{-8}

TABLE 4. Optimal design values related to the cases of Figure 4.

N	ψ_σ	$\tilde{h}_{min}$	$\Delta\tilde{h}_1$	$\Delta\tilde{h}_3$	$\tilde{V}$
3	3.33×10^{-4}	0.0165	0.0317	0.0058	1.13×10^{-3}
3	6.66×10^{-4}	0.0112	0.0233	0.0062	8.01×10^{-4}
3	1×10^{-3}	0.0099	0.0229	0.0087	7.95×10^{-4}

TABLE 5. Optimal design values related to the cases of Figure 4.

N	ψ_γ	$\tilde{h}_{min}$	$\Delta\tilde{h}_1$	$\Delta\tilde{h}_3$	$\tilde{V}$	$\psi_\gamma\tilde{V}$
3	4.17×10^{-6}	0.0096	0.0217	0.0086	7.73×10^{-4}	3.22×10^{-9}
3	8.33×10^{-6}	0.0099	0.0229	0.0087	7.95×10^{-4}	6.62×10^{-9}
3	1.66×10^{-5}	0.0106	0.0257	0.0088	8.37×10^{-4}	1.39×10^{-8}

TABLE 6. Combination of structural and load configurations to be considered for determining the range of parameters of the design abaci.

E GPa	γ kN/m^3	σ_{id} MPa	L m	q_0 kN/m	ψ_γ	ψ_σ	ψ_q
Concrete							
30	25	30	1	2	8.33×10^{-7}	1.00×10^{-3}	6.67×10^{-8}
30	25	30	10	2	8.33×10^{-6}	1.00×10^{-3}	6.67×10^{-9}
30	25	30	1	50	8.33×10^{-7}	1.00×10^{-3}	1.67×10^{-6}
30	25	30	10	50	8.33×10^{-6}	1.00×10^{-3}	1.67×10^{-7}
Timber							
8	5	30	1	2	5.63×10^{-7}	3.75×10^{-3}	2.50×10^{-7}
8	5	30	10	2	5.63×10^{-6}	3.75×10^{-3}	2.50×10^{-8}
8	5	30	1	50	5.63×10^{-7}	3.75×10^{-3}	6.25×10^{-6}
8	5	30	10	50	5.63×10^{-6}	3.75×10^{-3}	6.25×10^{-7}
Alluminium							
69	27	100	1	2	3.91×10^{-7}	1.46×10^{-3}	2.92×10^{-8}
69	27	100	10	2	3.91×10^{-6}	1.46×10^{-3}	2.92×10^{-9}
69	27	100	1	50	3.91×10^{-7}	1.46×10^{-3}	7.30×10^{-7}
69	27	100	10	50	3.91×10^{-6}	1.46×10^{-3}	7.30×10^{-8}
Steel							
210	78	250	1	2	3.71×10^{-7}	1.19×10^{-3}	9.52×10^{-9}
210	78	250	10	2	3.71×10^{-6}	1.19×10^{-3}	9.52×10^{-10}
210	78	250	1	50	3.71×10^{-7}	1.19×10^{-3}	2.38×10^{-7}
210	78	250	10	50	3.71×10^{-6}	1.19×10^{-3}	2.38×10^{-8}

TABLE 7. Combination of structural and load configurations to be considered for determining the range of parameters of the design abacus.

ψ_σ	ψ_q	h_{min}	$\Delta\tilde{h}_1$	$\Delta\tilde{h}_3$	$\Delta\tilde{h}_5$	$\tilde{V}$
0.5×10^{-3}	4.0×10^{-8}	0.0101	0.0223	0.0037	-0.0025	0.000858
	8.6×10^{-8}	0.0129	0.0341	0.0022	-0.0056	0.001290
	1.8×10^{-7}	0.0221	0.0482	0.0073	-0.0048	0.001838
	4.0×10^{-7}	0.0325	0.0705	0.0107	-0.0071	0.002695
	8.6×10^{-7}	0.0478	0.1032	0.0158	-0.0103	0.003955
	1.8×10^{-6}	0.0708	0.1508	0.0234	-0.0148	0.005810
	4.0×10^{-6}	0.1057	0.2192	0.0351	-0.0209	0.008551
1.0×10^{-3}	4.0×10^{-8}	0.0077	0.0163	0.0044	-0.0041	0.000781
	8.6×10^{-8}	0.0099	0.0209	0.0057	-0.0053	0.001006
	1.8×10^{-7}	0.0152	0.0321	0.0070	-0.0042	0.001311
	4.0×10^{-7}	0.0229	0.0499	0.0075	-0.0050	0.001904
	8.6×10^{-7}	0.0337	0.0731	0.0111	-0.0073	0.002794
	1.8×10^{-6}	0.0496	0.1070	0.0164	-0.0107	0.004102
	4.0×10^{-6}	0.0750	0.1567	0.0233	-0.0140	0.006033
1.5×10^{-3}	4.0×10^{-8}	0.0077	0.0163	0.0044	-0.0041	0.000781
	8.6×10^{-8}	0.0099	0.0209	0.0057	-0.0053	0.001006
	1.8×10^{-7}	0.0128	0.0269	0.0074	-0.0069	0.001298
	4.0×10^{-7}	0.0167	0.0350	0.0095	-0.0086	0.001675
	8.6×10^{-7}	0.0275	0.0597	0.0090	-0.0060	0.002280
	1.8×10^{-6}	0.0404	0.0875	0.0133	-0.0088	0.003347
	4.0×10^{-6}	0.0597	0.1279	0.0197	-0.0127	0.004917

List of Figures

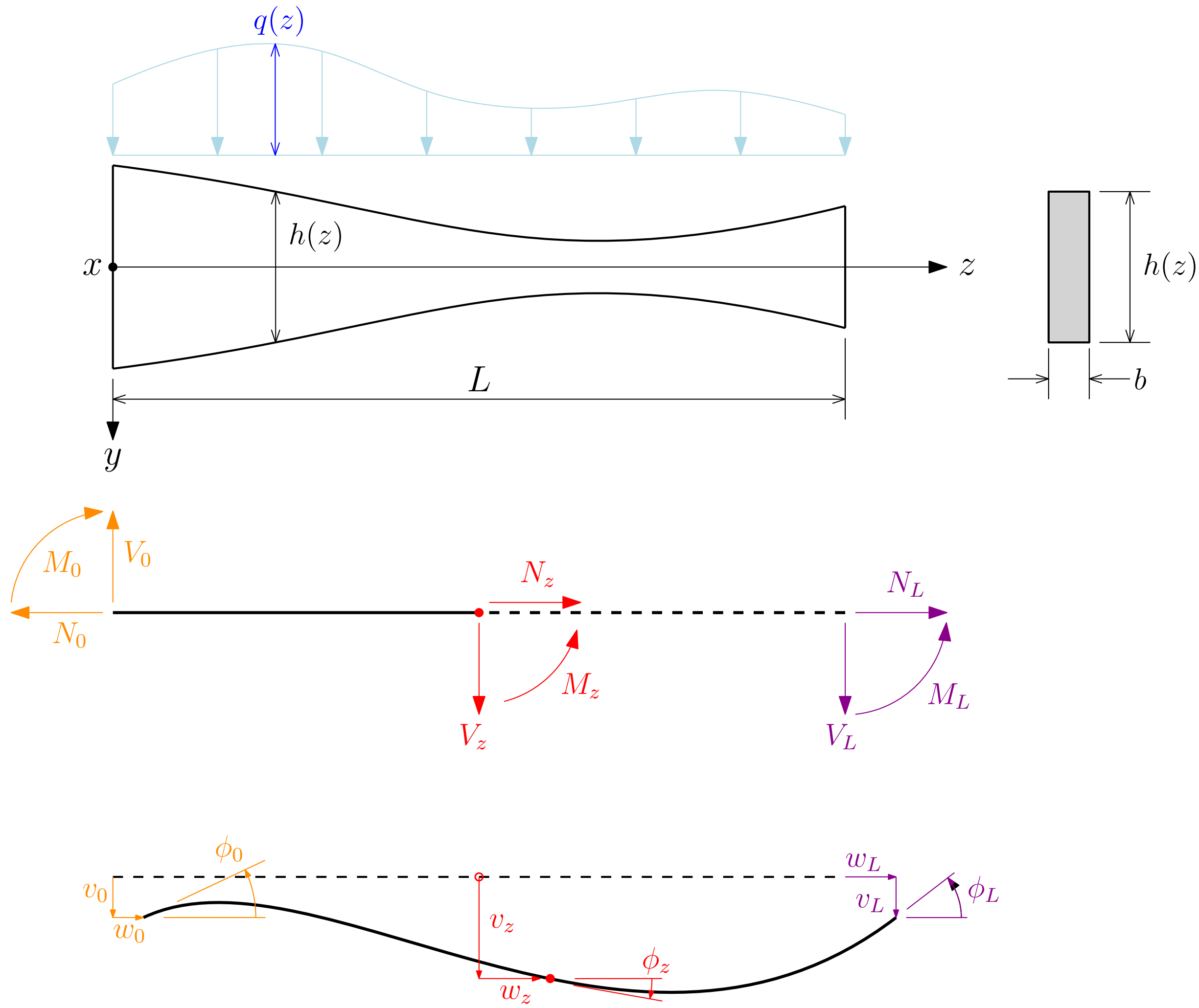

Fig. 1. Beam with variable cross-section: coordinate system, load, displacements, internal forces. The displacement field is denoted with components v, w, ϕ. The internal forces are N (axial), V (shear) and M (bending moment).

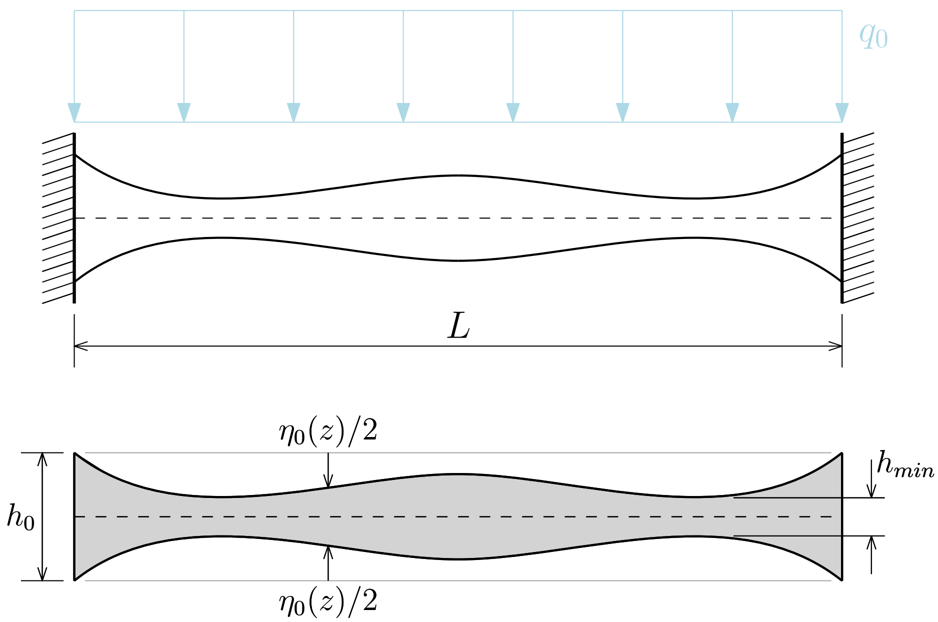

Fig. 2. Beam with variable cross-section generated with the emptying function of Eqn. (23).

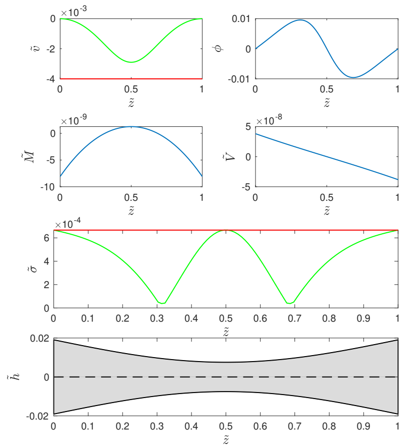

(a) One-lobe solution, $N = 1$

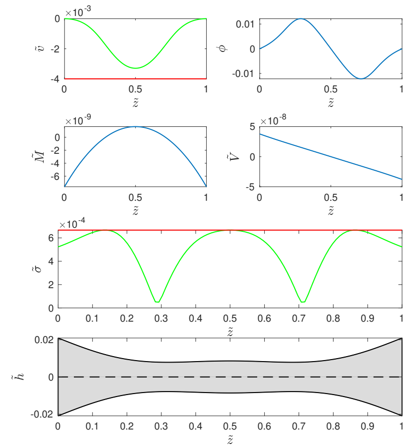

(b) Three-lobes solution, $N = 3$

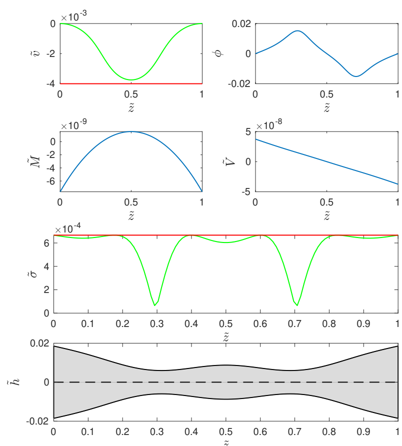

(c) Five-lobes solution, $N = 5$

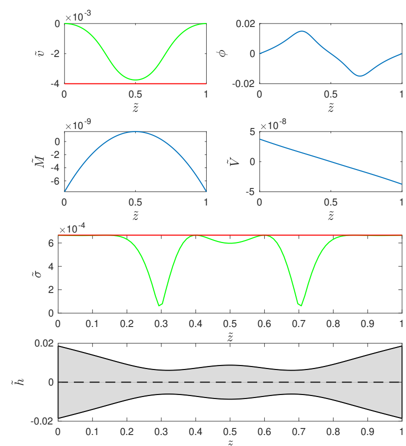

(d) Seven-lobes solution, $N = 7$

Fig. 3. Comparison of optimal beam solutions with variable cross-section considering different number of lobes. The parameters related to the weight per unit mass, the load and the maximum allowable stress are reported in Table 2.

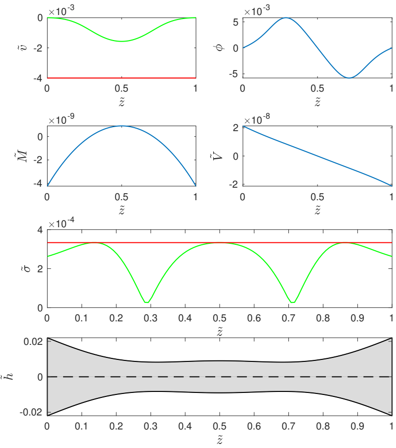

(a) $\psi_{\sigma} = 3.33 \times 10^{-4}$

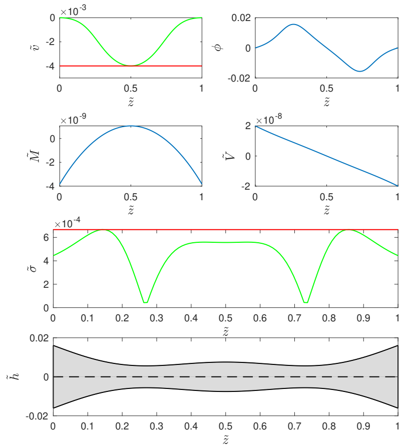

(b) $\psi_{\sigma} = 6.66 \times 10^{-4}$

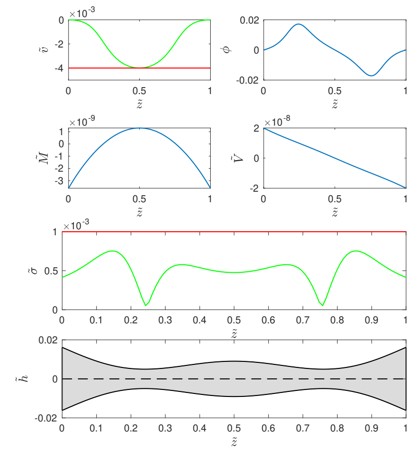

(c) $\psi_{\sigma} = 1 \times 10^{-3}$

Fig. 4. Comparison of optimal beam solutions of three-lobes variable cross-section considering different maximum stress levels, i.e. the value of parameter ψ_{σ}. The parameters related to the weight per unit mass, the load and the maximum allowable stress, as well as the optimal solution are reported in Table 4.

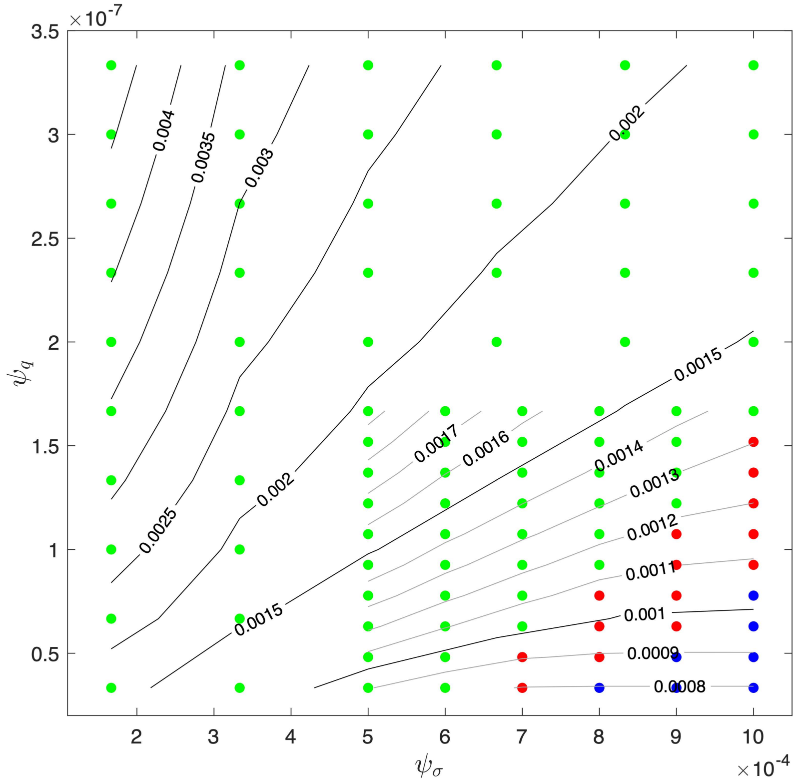

Fig. 5. Value of the dimensionless volume of the beam $\tilde{V}$ and binding solution constraints for different ψ_σ and ψ_q. The bullets indicate whether the relevant solution constraint is the maximum stress (green), Eqn. (21), the maximum displacement (blue), Eqn. (22), or both (red).

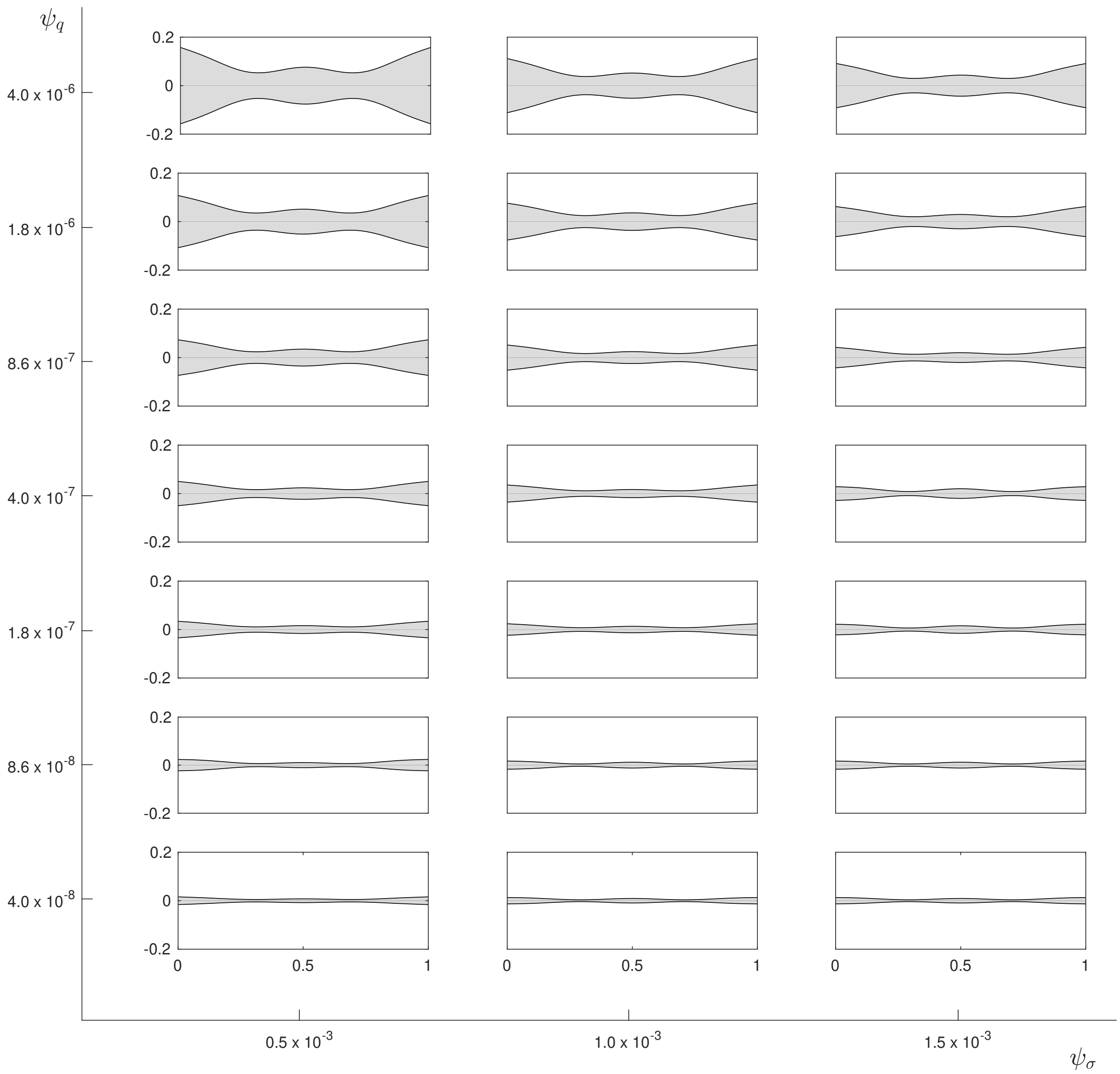

Fig. 6. Beam height profiles of the beams for various ψ_σ and ψ_q. The values of the design vector are reported in Table 7.